Title
Measuring precipitation kinetics of sparingly soluble salts using Shock-Freeze Cryo-TEM

Authors
Hendricks, U
Pascual, M Rodriguez
Banfield, JF
et al.

Publication Date
2015-12-01

DOI
10.1016/j.jcrysgro.2015.09.017

Peer reviewed

Journal of Crystal Growth 432 (2015) 108–115

Contents lists available at ScienceDirect

Journal of Crystal Growth

journal homepage: www.elsevier.com/locate/jcrysgro

Measuring precipitation kinetics of sparingly soluble salts using Shock-Freeze Cryo-TEM

U. Hendricks [a], M. Rodriguez Pascual [a], J.F. Banfield [b], A.E. Lewis [a,*]

[a] Department of Chemical Engineering, University of Cape Town, Rondebosch, Cape Town 7700, Western Cape, South Africa
[b] Earth & Planetary Science, University of California, Berkeley, 307 McCone Hall, Berkeley, CA 94720-4767, United States

ARTICLE INFO

Article history:
Received 17 April 2015
Received in revised form
27 August 2015
Accepted 5 September 2015
Communicated by Y. Furukawa
Available online 28 September 2015

Keywords:
A1. Nucleation
A1. Shock-Freeze Cryo-TEM
A1. Y-mixer
A2. Industrial crystallisation
B1. Barium compounds

ABSTRACT

The precipitation of barium sulphate in a rapid mixing device (Y-mixer) coupled with an instantaneous sample freezing device was studied in order to accurately measure the nucleation rate. In this Shock-Freeze Cryo-TEM (SFCT) approach, a small volume of solution was removed from the stream directly into liquid ethane by means of a gravitational guillotine. Using different pipe lengths to measure various residence times, it was possible to determine the particle size, morphology, numbers of primary particles and thus nucleation rate. The nucleation rates were found to be a strong function of Reynolds number, up to $Re = 3 \times 10^4$ (Re being inversely related to the micromixing time). The measured nucleation rates ranged between 2.79×10^{14} and 3.81×10^{17} # m^{-3} s^{-1} at supersaturations between 4×10^6 and 1×10^8. The measured particle sizes in this work (ranging from 62 to 320 nm for supersaturation values between 4×10^6 and 1×10^8) were smaller than those measured by previous researchers, possibly because previous work did not quench the reaction sufficiently fast and thus allowed the particles a longer time to increase in size. In summary, this work successfully achieved a fast, accurate and reproducible nucleation rate measurement that could also give information about particle morphology.

1. Introduction

Reactive precipitation is used extensively in the pharmaceutical and fine chemical industries as well as in the mining sector. Salts that are sparingly soluble are also commonly encountered in hydrometallurgical systems [1–3] and are also important in many natural environments. Precipitation as a purification and separation process offers the advantages of high product yield but has the disadvantage of forming products with undesirable properties, such as small particle sizes, and thus there are usually difficulties in separation and downstream processing. These particle properties are a function of the particle structure, morphology and particle size distribution, and can be influenced by manipulating the conditions of the precipitation reaction. The link between the processing conditions and the product properties can be obtained by understanding as well as measurement of the kinetic processes that occur during precipitation [4].

2. Precipitation and nucleation

Precipitation can be divided into several sub-processes: the primary processes being nucleation and growth, and the secondary processes being agglomeration, attrition and dissolution [5]. The nucleation process begins with the stochastic appearance of nanoscopically-sized molecule clusters in the solvent. Primary nucleation can be initiated through the spontaneous stochastic formation of nuclei (homogeneous nucleation) or by the attachment of the nuclei on existing particles (heterogeneous nucleation) [6,7]. In a precipitation process, the supersaturation of the ionic species in solution with respect to the solid phase is the driving force for nucleation and growth of a precipitate. Since the supersaturation for sparingly soluble salts is usually high, the precipitation process is dominated by nucleation [8,9]. Measuring the nucleation rate of low solubility compounds as a function of supersaturation is challenging because nucleation occurs extremely quickly at the very high supersaturations that are generated by the reaction.

3. Previous nucleation rate measurement methods

The current methods of measuring nucleation rates include both sampling and *in situ* techniques. Roelands and co workers [10] used both T and Y-shaped devices to mix the reagents and to initiate precipitation. The length of the reaction tube leaving the T-mixer and the fluid velocity in the outlet pipe was used to determine the residence time of the reaction. In order to arrest the precipitation process at the end of the reaction tube, the solution was directed into a quenching container that contained a large

* Corresponding author. Tel.: +27 21 650 4091.
E-mail address: Alison.Lewis@uct.ac.za (A.E. Lewis).

http://dx.doi.org/10.1016/j.jcrysgro.2015.09.017

volume of deionized water. After the reaction was quenched, a dynamic light scattering technique was used to measure the number of particles and size of the particles for the specified supersaturation. However, it is known that this kind of quenching step is not rapid enough to stop the precipitation reaction from progressing.

Judat and Kind [11] used two methods: firstly, a Y-shaped mixing device followed by a quench of the free jet in a beaker with distilled water in an attempt to stop any further growth and aggregation. However, this method was unable to prevent further crystal growth. The second quenching method used a TEM grid that was moved through the jet with a speed of approximately 13 m s^{-1} and was thus able to shock freeze the jet within about 5 ms after sampling. However, numerous difficulties were experienced with this elaborate measurement technique, including destruction of the copper film on the TEM grid by the high jet velocities and the low temperatures; thickness of the ice layer being too thick for electron beam transmission as well as thickness of the ice layer being too thin and thus sublimating under the low pressure inside the microscope. Kugler and co-workers [12] used *in situ* synchrotron radiation wide angle x-ray scattering (WAXS) to measure the particle number as a function of supersaturation for stoichiometric precipitation of barium sulphate. Nonetheless, they were not able to calculate nucleation rates from experimental data due to the extremely short time periods required.

Roelands and co-workers [13] analysed and reviewed methods for the measurement of nucleation rates in precipitation processes and concluded that measurement of homogenous nucleation rates (such as those experienced during the precipitation of sparingly soluble salts) requires a method that takes into account the depletion of supersaturation down the length of the mixing tube, a method of instantaneous mixing and a particle counting technique that is number based.

In summary, it is clear that previous methods are not able to provide accurate and repeatable nucleation rate measurements. Therefore, nucleation measurement techniques are moving towards online, *in situ* and/or extremely rapid measuring techniques, which have the ability to measure nucleation rates of rapidly precipitating salts. The *in situ* methods provide high quality experimental data since no quenching is required. Most of these techniques use light scattering or interfering techniques. Some of these techniques such as Focused Beam Reflectance Measurements (FBRM) [14], Small-Angle X-ray Scattering (SAXS) [15] and Digital Holographic Microscopy (DHM) [16] can be used to determine the number and size of particles that are formed during precipitation reactions [16–18]. In contrast, the rapid measuring techniques attempt to speed up the quenching step sufficiently for accurate measurement. However, for both techniques, the limitations lie in the ability to detect the extremely small particles as well as in the ability to provide sufficiently fast micromixing times.

4. Proposed nucleation rate measurement method

It is the intention of this work to present and evaluate a technique for measuring nucleation rates that, although not strictly *in situ*, satisfies the requirement of being able to capture the nucleation information extremely rapidly. Thus, we proposed that it might be suitable, not only for measuring the nucleation rates of the model substance ($BaSO_4$), but of a much broader range of sparingly soluble salts.

In this study, the nucleation rates of $BaSO_4$, (formed using $BaCl_2$ and Na_2SO_4 (Eq. (1))) and which has a solubility product (K_{sp}) of 1.1×10^{-10} [19], were investigated at several supersaturation values. This particular precipitation reaction was chosen because of the relatively low solubility of $BaSO_4$, as well as the fact that only one polymorph is formed. In addition, extensive nucleation rate data exists for barium sulphate and therefore comparisons can be made between the literature and the data measured in this study [20–22].

$$BaCl_2 + Na_2SO_4 \rightarrow BaSO_4 + NaCl \quad (1)$$

Due to the exceedingly small size of the nuclei clusters and rapid rate with which nucleation occurs, a combination of a Y-mixer for rapid micromixing and a Cryo-TEM system was used. The Cryo-TEM system was adapted by adding a guillotine and shock freezing with liquid ethane to enable the experimental determination of the number of nuclei as a function of residence time. The morphology and size of the crystals can be accurately measured using this method. The theoretical micromixing time in the Y-mixer can be calculated using Eq. (2), as proposed by Judat and Kind [11], but originally proposed by Baldyga and Bourne [23]:

$$\tau_m = \frac{12}{\ln 2}\left(\frac{\nu}{\epsilon}\right)^{1/2} \quad (2)$$

where τ_m = micromixing time (s)
ν = kinematic viscosity ($m^2\ s^{-1}$)
ε = turbulent energy dissipation rate ($m^2\ s^{-3}$)

The turbulent energy dissipation rate was calculated, as recommended by Roelands and co-workers [24], from an estimate of the pressure drop over the outlet tube of the Y-mixer, according to:

$$\varepsilon = \frac{\phi_v \Delta P}{\rho V} = \frac{2fU^3}{D} \text{ with } 4f = 0.316Re^{-0.25} \quad (3)$$

where ε = mean turbulent kinetic energy dissipation rate ($m^2\ s^{-3}$)
Φ_v = flow rate (m s^{-1})
ΔP = pressure drop over the mixer (N m^{-2})
ρ = density of fluid (kg m^{-3})
V = volume of outlet tube (m^3)
f = friction factor for the tube wall
U = average flow velocity (m s^{-1})
D = internal diameter of outlet tube (m)

For this system, the micromixing times are calculated using the constants in Table 1 and were found to be between 1×10^{-6} and 1×10^{-2} s.

Experimentally, the nucleation rate (J) can be calculated by measuring the change in the number of particles with time (t).

$$J(t) = \frac{dN_t}{dt} \quad (4)$$

Integrating Eq. (4) [7] gives

$$N_t = N_0 + JVt \quad (5)$$

where N_t = number of particles at time = t (#)
N_0 = number of particles initially in the solution (#)
J = nucleation rate [# $m^{-3}\ s^{-1}$]
V = volume of the system (m^3)
t = residence time (s)

Thus, if N_t is plotted against t, the resulting straight line will have a gradient of J, the nucleation rate, and an intercept at N_0, the initial number of particles. According to Classical Nucleation Theory (CNT), the nucleation rate is a strong function of supersaturation, and can

Table 1
Constants used to calculate micro-mixing times.

Internal diameter of outlet tube (m)	0.004
ν, kinematic viscosity ($m^2\ s^{-1}$)	1×10^{-6}
Reynolds number	2×10^4–3.4×10^4
ϵ, (mean turbulent kinetic energy dissipation rate) ($m^2\ s^{-3}$)	2×10^3–5×10^5
τ_m (s)	1×10^{-6}–1×10^{-2}

be calculated using Eq. (6) [24]

$$J = A S \exp\left(-\frac{B}{\ln^2 S}\right) \quad (6)$$

where S = supersaturation;
A = the supersaturation independent kinetic parameter;
B = dimensionless thermodynamic parameter.

According to Roelands [24], the pre-exponential kinetic parameter, A, gives information as to whether the nucleation occurs homogeneously or heterogeneously whereas the exponential factor B, incorporates the effect of the interfacial energy between crystal and solution.

The supersaturation is a function of the solubility of the precipitating salt and is calculated as follows [7]:

$$S = \frac{a_+ a_-}{K_{sp}} \quad (7)$$

where a_+ = the activity of the cation in solution;
a_- = the activity of the anion in solution;
K_{sp} = the solubility product of the precipitating solute.

5. Experimental

5.1. Reagents

The reagents used were supplied by Merck and consisted of analytical grade (99.9% purity) barium chloride and sodium sulphate.

5.2. Shock-Freeze Cryo-TEM

The experiments were performed using a Y-mixer with internal diameters of the inlet and outlet tubing of 4 mm (Fig. 1). Solutions were prepared using deionized water and feed solutions were maintained at 25 °C in two individual stirred tanks. Two magnetic drive gear pumps were set up so that they provided a constant flow of reagents to the Y-mixer.

The stream of mixed reagents was shock frozen using liquid ethane, which was maintained at a temperature of −180 °C (see Fig. 2). A guillotine was used to slice through the frozen Y-mixer at different exit tube lengths. At the tip of the guillotine, an attached carbon template collected samples that were maintained in the frozen state and then analysed using CRYO-Transmission Electron Microscopy (TEM). Using TEM, it was possible to observe the size, morphology and number of particles per unit volume. The shock freezing prevented further nucleation and growth of the particles, thus providing representative nucleation kinetics for the residence time being investigated.

5.3. Experimental procedure

For all nucleation rate experiments, the guillotine was used to take samples of the reaction stream for residence times of 0.0035, 0.007 and 0.0093 s, which corresponds to pipe lengths of 0.03, 0.06 and 0.08 m. In order to determine the nucleation rate, experiments were carried out in triplicate and 10 TEM images were taken for each sample. The number of particles was measured from TEM images and the relevant magnification was used to determine the number of particles per m^3 of volume. From this, the nucleation rate (# $m^{-3}\,s^{-1}$) was determined, based on the residence time at which the sample was taken. Agglomeration was not observed, partly due to the very short residence times, since agglomeration is a secondary process. Although some of the TEM images did seem to exhibit "clustering together" of particles, in order for this to be evidence of agglomeration, there would need to be the presence of smaller particles as well. The absence of these particles in the samples has led to the deduction that agglomeration does not occur. Therefore, each complex particle was counted as a single nucleation event.

5.3.1. Verification of shock freeze step

In order to verify the quenching ability of the shock-freeze step in the experimental setup, TEM images were taken of samples using the guillotine at a residence time of 0.003 s and for a barium sulphate of concentration of 0.02 M, both with and without the liquid ethane being used for shock freezing.

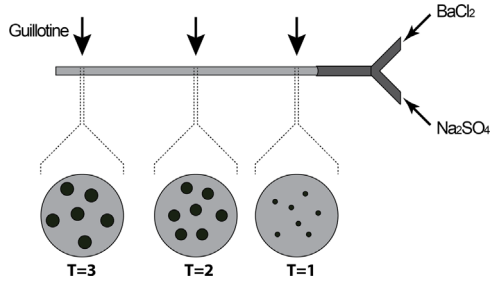

Fig. 2. Schematic representation of the effect of the different Y-mixer exit pipe lengths on residence times.

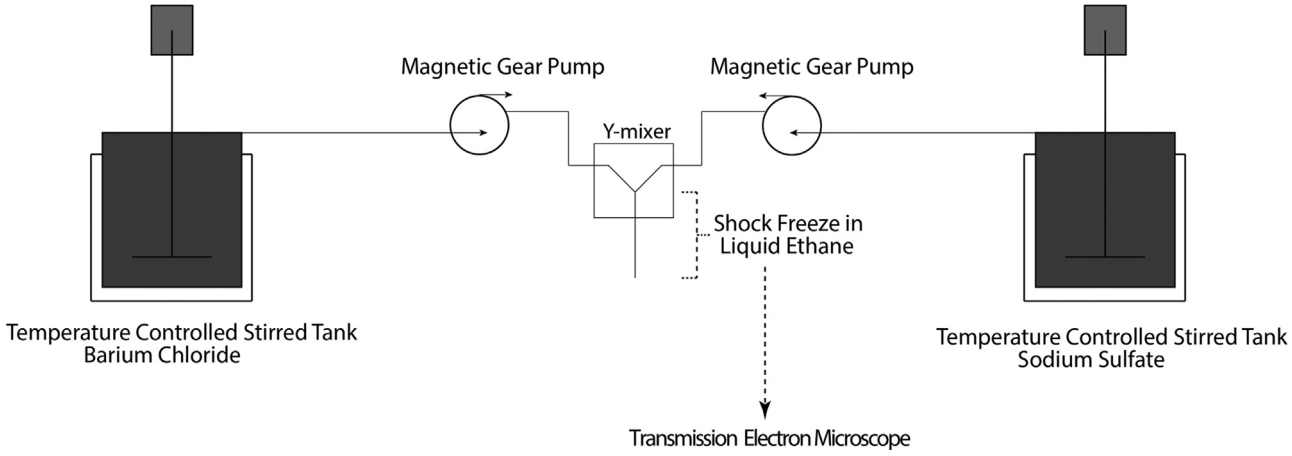

Fig. 1. Shock-Freeze Cryo-TEM experimental setup.

5.3.2. Establishing the minimum flow rate for the nucleation experiments

In order to establish the *minimum* required flow rate for the nucleation rate experiments, nucleation rates for the barium sulphate system at concentrations of 0.02, 0.035 and 0.05 M were experimentally determined using Shock-Freeze Cryo-TEM at five different volumetric flow rates, all listed in Table 2.

5.3.3. Nucleation rate experiments

All subsequent nucleation rate experiments were carried out using a flow rate of 108 ml s^{-1} *i.e* at a Reynolds number of 3.4×10^4. The nucleation rates for barium sulphate at concentrations of 0.02, 0.05, 0.06, 0.08 and 0.1 M were investigated using the Shock-Freeze Cryo-TEM experimental setup.

6. Results and discussion

6.1. Verification of the shock freeze step

In Fig. 3, the effectiveness of shock freezing for capturing an instantaneous snapshot of number and size of particles at a specific stage of nucleation is demonstrated at a concentration of 0.02 M. Two experiments were conducted at the same conditions: the one without and the one with shock freezing. In the case of "without shock freezing", the chamber was cooled down and the sample was transferred frozen. In the case of "with shock freezing", the method described in the earlier section was followed. In the left hand image (A), there are orders of magnitude more particles observable than on the right (B). Without shock freezing, nucleation continues to occur after the sample is taken and therefore the number of particles measured is not representative of the residence time specified in the experiment. The shock-freezing step effectively arrests the experiment at the moment that the sample is taken, and thus provides a representative measurement of the nucleation rate at that residence time.

Table 2
Volumetric flow rates used to establish the minimum required flow rates for nucleation rate measurements.

Volumetric flow rate (ml s^{-1})	Flow velocity (m s^{-1})	Reynolds number
10.8	0.86	3.4×10^3
30.2	2.41	9.6×10^3
54.0	4.30	1.7×10^4
97.2	7.73	3.1×10^4
108.0	8.59	3.4×10^4

6.1.1. Establishing the minimum flow rate for the nucleation experiments

Fig. 4 shows how the measured number of particles, and thus the measured nucleation rate, increases with an increase in Reynolds number. Each of the images was recorded at the same residence time. The samples were taken at different tube lengths to accomplish this.

It is clear that the liquid-to-solid conversion in these experiments was not constant, but because the initial supersaturation was extremely high, and the experiments were arrested before very much mass had been produced, the mean supersaturation was assumed to remain essentially the same.

The measured nucleation rate as a function of the Reynolds number is presented in Fig. 5. It can be seen that, as the Reynolds number increases to 3.1×10^4, the nucleation rate reaches a maximal plateau and thus it can be said that the limiting Reynolds number has been reached. At this point, mixing is sufficiently fast such that the nucleation rate is no longer influenced by it. Thus, the measured kinetics can be assumed to be the kinetics of the precipitation process and not the kinetics of the mixing process.

Fig. 6 illustrates how the particle size and morphology change as the Reynolds number increases, from larger, twinned or radial growth dendritic shapes at $Re = 3.4 \times 10^3$ to much smaller sizes and less twinning at $Re = 3.4 \times 10^4$. Quite extensive clustering of the particles is observed at the lower *Re* numbers, but this is much less evident at the highest Reynolds number of $Re = 3.4 \times 10^4$ in image D of Fig. 6. Since this is the Reynolds number at which the measurements were carried out, clustering is not discussed further.

Fig. 7 quantifies graphically the effect of Reynolds number on particle size. From the figure, it is clear that, as the Reynolds number increases from 3.4×10^3 to 1.7×10^4, the average particle size rapidly decreases. However, between Reynolds numbers of 3.1×10^4 and 3.4×10^4, the particle size remains relatively unchanged.

This behaviour can be accounted for as follows: as the Reynolds number increases, the micromixing is faster, and thus there is an *increase* in the local supersaturation experienced by each particle, thereby favouring nucleation over growth. Therefore, at the higher Reynolds numbers, the particles are measurably smaller. However, between the Reynolds numbers of 3.1×10^4 and 3.4×10^4, there is a negligible decrease in particle size. With reference to Fig. 5, it can also be seen that, between the Reynolds numbers of 3.1×10^4 and 3.4×10^4, there is a very small change in particle number.

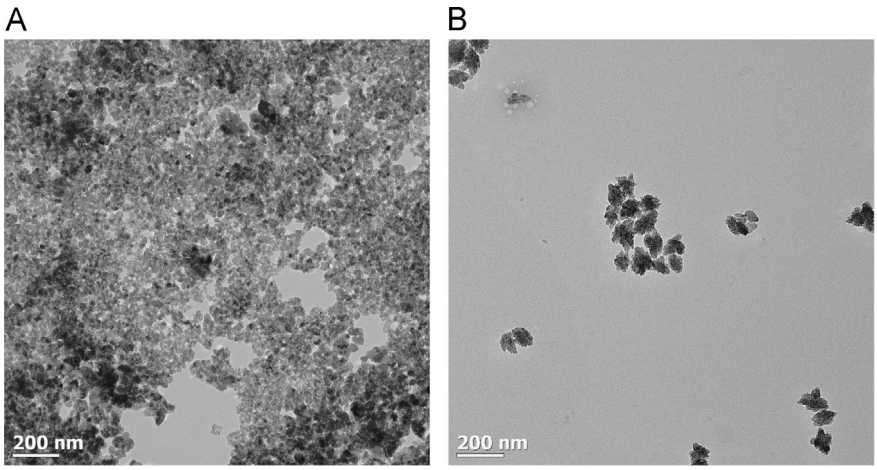

Fig. 3. Effect of shock freezing on the number of particles generated (A) without shock freezing using liquid ethane and (B) with shock freezing using liquid ethane.

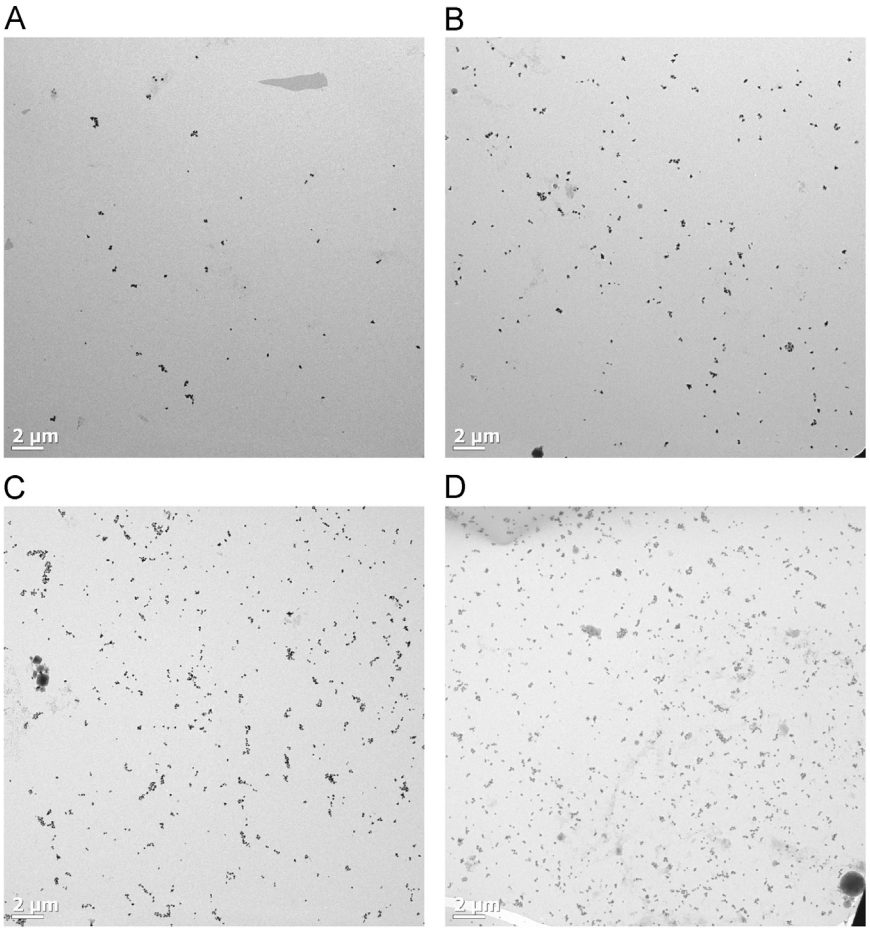

Fig. 4. Images for Reynolds numbers of (A) 3.4×0^3, (B) 9.6×10^3, (C) 1.7×10^4 and (D) 3.1×10^4 show an increase in the number of particles as the Reynolds number is increased.

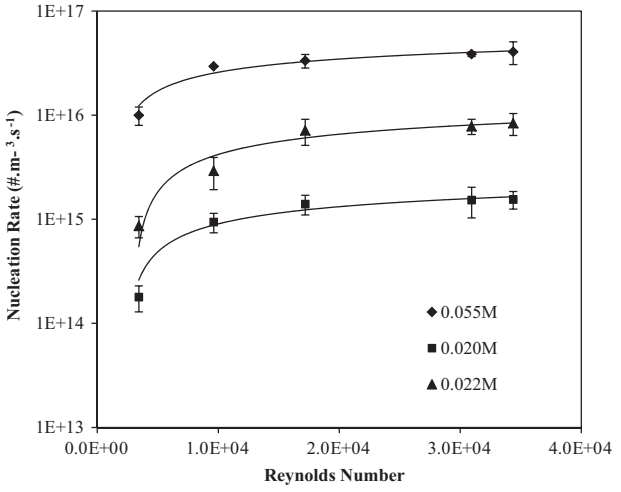

Fig. 5. Nucleation rates as a function of Reynolds number for barium sulphate precipitation.

Therefore, it was concluded that sufficiently effective mixing has been achieved at the higher Reynolds number and thus, for this system, the nucleation rate measurements were carried out at $Re=3.4\times10^4$.

6.1.2. Nucleation rate measurements

As a result of the mixing time experiments above, all the nucleation rate experiments were carried out at a Reynolds number of 3.4×10^4, in order to ensure that sufficiently fast mixing was achieved. Table 3 shows the nucleation rates measured for the range of supersaturation values investigated.

Under these conditions of extremely high supersaturation and rapid mixing, the waiting time for nucleation (the induction time) has been assumed to be negligible. This is confirmed by the work of Roelands [24,13]. For the same reasons, the type of nucleation is almost certainly homogenous, as confirmed by the work of Nielsen [21], who found that, for the barium sulphate systems, above 0.01 M, homogeneous nucleation dominated. For this work, the lowest concentration studied was 0.02 M, and therefore all the results presented are in the homogenous nucleation region. In addition, when using the data in Table 3 to calculate the parameters A and B in Eq. (6), the calculated value for A (8.02×10^{30} m^{-3} s^{-1}) is consistent with that for homogeneous nucleation, as discussed by Roelands [13].

When the nucleation rate data for barium sulphate in this work is compared with that previously measured by Nielsen [25], Mohanty [26] and Taguchi [27], it can be seen the nucleation rates measured in this work are somewhat lower than those measured by previous researchers, as demonstrated in Fig. 8. This can possibly be attributed to the experimental method by which the previous data were obtained. Nielsen used a 2L separation funnel to collect the stream as it exited the mixer and the particles were counted under a microscope some time later. Gelatin, carboxymethylcellulose and sodiumpyrophosfate were used as peptizing agents to prevent coagulation of the particles and thus to prevent further nucleation and growth [8]. Mohanty discharged the reacting stream directly into a 50–500 ml gelatine solution and subsequently placed a sample onto a microscope slide for counting

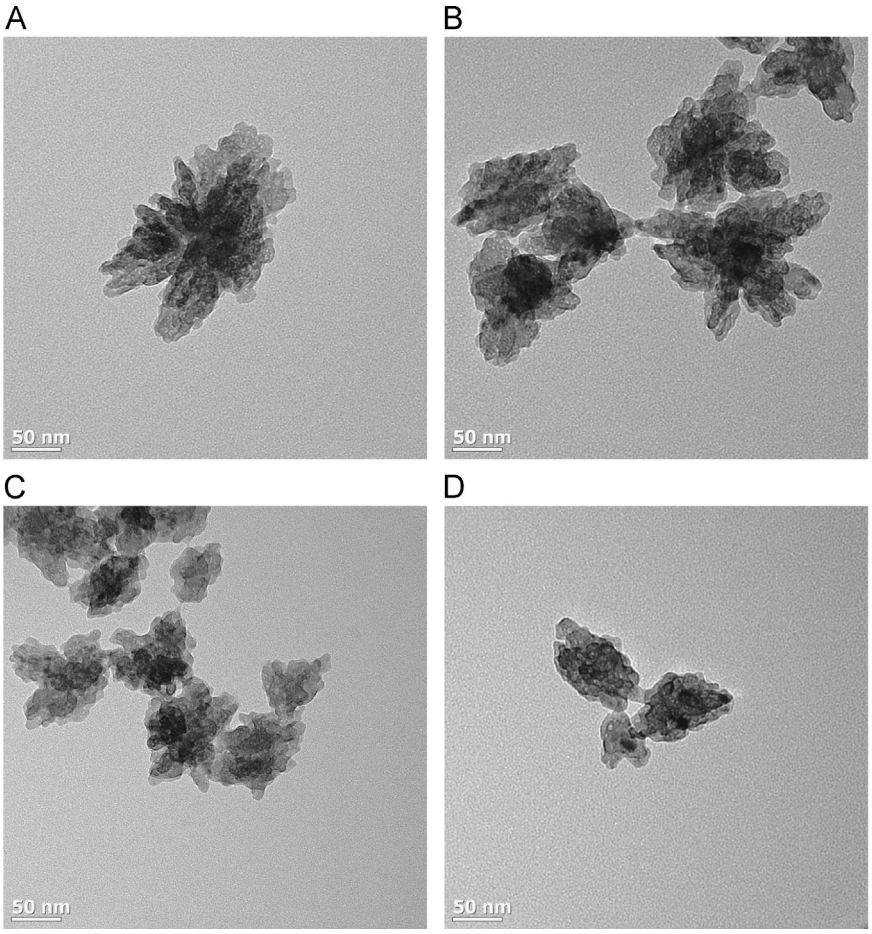

Fig. 6. Bright field TEM images showing the barium sulphate particles produced at different Reynolds numbers. (A) 3.4×10^3, (B) 9.6×10^3, (C) 1.7×10^4 and (D) 3.4×10^4.

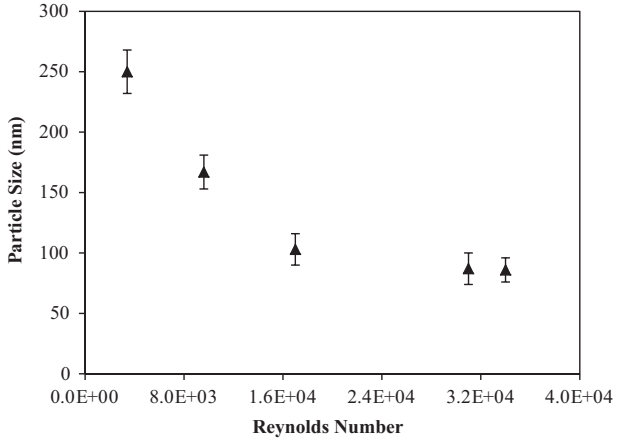

Fig. 7. Particle size as a function of Reynolds number. (A) 3.4×10^3, (B) 9.6×10^3, (C) 1.7×10^4, (D) 3.1×10^4 and (E) 3.4×10^4.

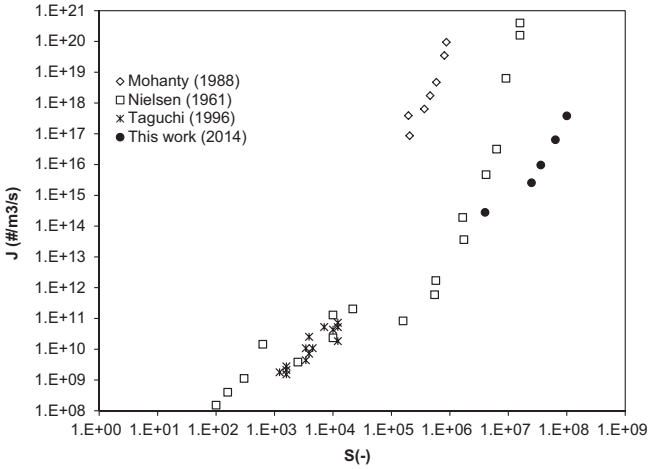

Fig. 8. Nucleation rate *versus* supersaturation ratio.

Table 3
Experimentally determined nucleation rates for a range of supersaturation values.

Experiment no.	Supersaturation	Nucleation rates	Concentration
		(# $m^{-3} s^{-1}$)	(M)
1	4.0×10^6	2.79×10^{14}	0.02
2	2.5×10^7	2.55×10^{15}	0.05
3	3.6×10^7	9.63×10^{15}	0.06
4	6.4×10^7	6.39×10^{16}	0.08
5	1.0×10^8	3.81×10^{17}	0.10

of the particles. During this time, many new particles may have formed, resulting in an artificially high nucleation rate. Taguchi and co-workers conducted a series of batch experiments and used an off-line zone sensing particle size analyser to measure the particle sizes [27]. Fig. 8 summarises these observations but illustrating that previously, nucleation rates 100 to 1000 times the more recently measured value were observed.

The effect of the supersaturation on the average sizes of the particles is illustrated in Fig. 9 and given quantitatively in Fig. 10. Both of these figures illustrate how the average size of the particles decreases as the supersaturation of the system is increased.

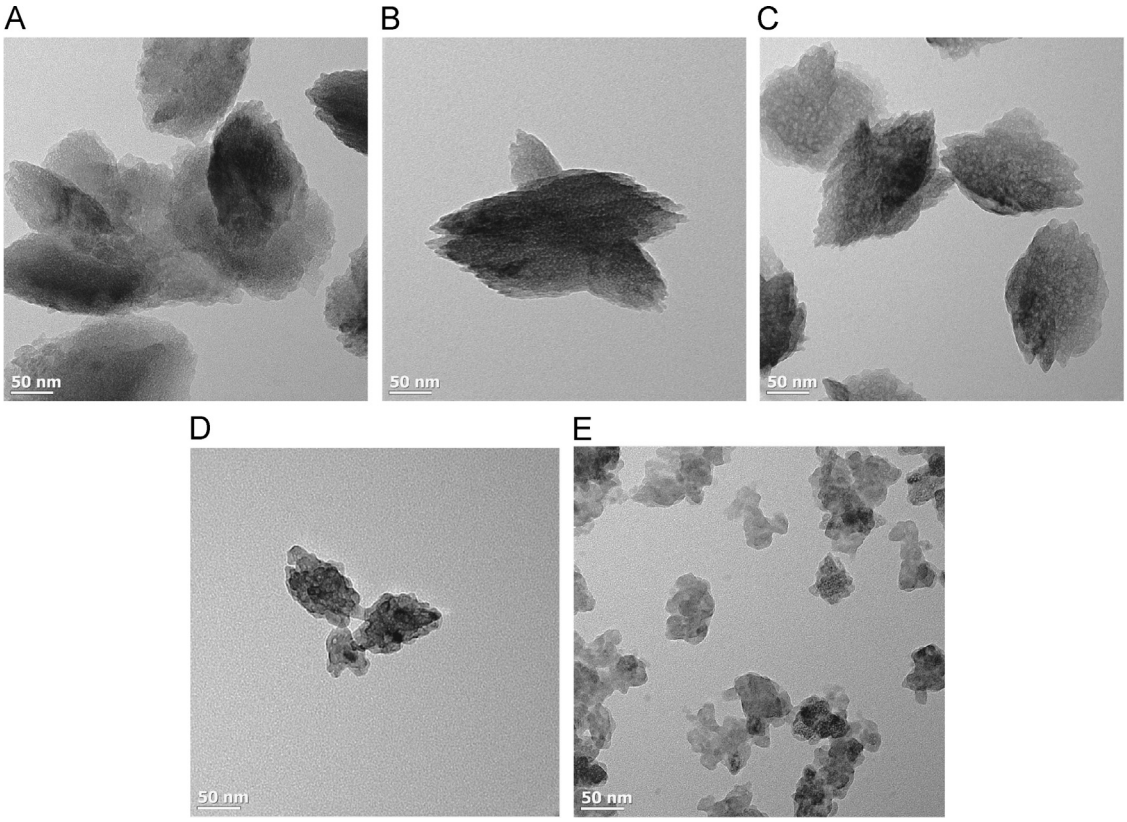

Fig. 9. Effect on particle size for supersaturation values of (A) 4.0×10^6, (B) 2.5×10^7, (C) 3.6×10^7, (D) 6.4×10^7 and (E) 1.0×10^8.

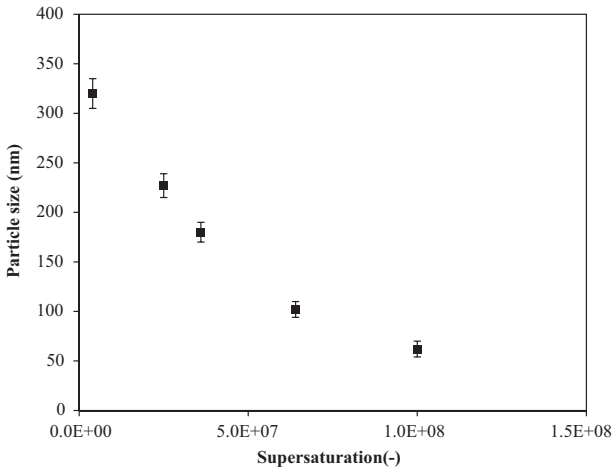

Fig. 10. Effect of supersaturation on particle sizes measured using TEM.

From Fig. 9, it is apparent that, at the lower supersaturation values, the particles are larger and less numerous, indicating that besides nucleation, growth is also occurring. As the supersaturation is increased, the number of particles in the frame increases and the measured size decreases. The morphology of the particles does not change significantly over the range of measured supersaturation, indicating that once nucleation has occurred, further decreases in supersaturation levels are due to crystal growth.

From Fig. 10, it can be seen that, as the supersaturation is increased from 4.0×10^6 to 1.0×10^8, the measured particle size decreases from 320 nm at the lower supersaturation to 62 nm at the highest supersaturation. This is in contrast to the data collected by previous researchers, who measured particle sizes somewhat larger than those measured in this study. Mohanty, for example, measured particle sizes of $>1\,\mu m$ from TEM images taken of the samples for the same supersaturation values used in this study [26]. This is an indication that, in previous experiments, growth of the particles was possibly not sufficiently inhibited. In this study, for the same supersaturation range used by Mohanty, much smaller particle sizes were measured.

Both Figs. 9 and 10 illustrate how the average size of the particles decreases as the supersaturation of the system is increased. This is due to the fact that, with increased supersaturation, the nucleation mechanism dominates and thus nucleation is favoured over growth.

7. Conclusions

By using a rapid mixing device coupled to a shock-freeze system which prevented further nucleation and growth, it was possible to accurately measure the nucleation kinetics of a precipitation reaction. The Cryo-TEM system allowed investigation of the morphology of the produced particles. Based on the results of the mixing experiments, the limiting Reynolds number (*i.e* the Reynolds number below which the results were mixing limited) was 3.4×10^4. The particle size decreased from 250 to 86 nm as the Reynolds number was increased from 3.4×10^3 to 3.4×10^4, indicating an increase in the supersaturation due to improved mixing.

The nucleation rates ranged from 2.79×10^{14} to 3.81×10^{17} for supersaturation values ranging from 4×10^6 to 1×10^8. Nucleation rates obtained using Shock-Freeze Cryo-TEM are a few orders of magnitude less than data obtained by Nielsen [21], Mohanty [26] and Taguchi [27]. We attribute this difference to our experimental approach, which ensured proper quenching of the precipitation process, thus accurate nucleation rate measurements. This impacts nucleation kinetic and thermodynamic analyses. From the TEM

images we see that the particle size decreased from 320 to 62 nm with increasing supersaturation from 4.0×10^6 to 1.0×10^8 as a result of nucleation being favoured over growth.

This work shows that, without using liquid ethane to shock-freeze the precipitating process, new particles had time to form, causing inaccurate nucleation rates to be calculated for the residence times being investigated. However, Shock-Freeze Cryo-TEM provides an accurate and repeatable experimental method for characterizing precipitation kinetics of rapidly precipitating systems such as sparingly soluble salts. Inhibition of the precipitation reaction was achieved. A high level of accuracy in the measurement of particle size improved the resolution of the early nucleation process, which was impossible using methods that provide only micron-scale resolution.

In future work, the techniques will be used to measure the number and size of particles for longer residence times, which will assist in the understanding of both nucleation and growth mechanisms for a range of sparingly soluble salt systems. This will provide valuable insight into the relative importance of classical atom-by-atom growth *versus* particle attachment-based crystal growth (for example, oriented attachment [28]). In addition, the technique will be extended to investigate the precipitation kinetics of a range of other sparingly soluble salts.

Acknowledgements

Grateful thanks are due to the National Research Foundation of South Africa (Grant no. 73678), who partially funded this work.

References

[1] D.R. Weir, D.G.E. Kerfoot, H.C. Scheie, Removal of selenium from acidic copper sulphate solutions, United States Patent Number CA 1139258 A1, 1983.
[2] T.P. Mokone, R.P. van Hille, A.E. Lewis, Effect of solution chemistry on particle characteristics during metal sulfide precipitation, J. Colloid Interface Sci. 351 (2010) 10–18.
[3] A. Lewis, M. Mangere, Reactive crystallization of copper selenide at very high supersaturation: a challenge to classical crystallization theory for sparingly soluble salts, Chem. Eng. Technol. 34 (4) (2011) 517–524.
[4] R. Zauner, A.G. Jones, Determination of nucleation, growth, agglomeration and disruption kinetics from experimental precipitation data: the calcium oxalate system, Chem. Eng. Sci. 55 (19) (2000) 4219–4232.
[5] A. Mersmann, Crystallization Technology Handbook, 2nd ed., Marcel Dekker, New York, 2001.
[6] D. Kashchiev, Nucleation: Basic Theory with Applications, 1st ed., Elsevier Science, Oxford, 2000.
[7] D. Kashchiev, G.M. van Rosmalen, Review: nucleation in solutions revisited, Cryst. Res. Technol. 38 (7–8) (2003) 555–574.
[8] C.Y. Tai, Experimental techniques for identifying operating variables of crystal growth and nucleation – from readily soluble salts to sparingly soluble salts, J. Taiwan Inst. Chem. Eng. 40 (6) (2009) 682–688.
[9] C.Y. Tai, P.C. Chen, C.C. Chen, Particle nucleation and growth, in: A. Hubbard (Ed.), Encyclopedia of Surface and Colloid Science, Marcel Dekker, New York, 2002.
[10] C.P.M. Roelands, R.R.W. Roestenberg, J.H. ter Horst, H.J.M. Kramer, P.J. Jansens, Development of an experimental method to measure nucleation rates in reactive precipitation, Cryst. Growth Des. 4 (5) (2004) 921–928.
[11] B. Judat, M. Kind, Morphology and internal structure of barium sulfate – derivation of a new growth mechanism, J. Colloid Interface Sci. 269 (2) (2004) 341–353.
[12] R. Kugler, S. Doyle, M. Kind, Precipitation kinetics of barium sulfate at high supersaturation by in-situ synchrotron radiation WAXS, in: Proceedings of the International Symposium on Industrial Crystallization, 16–19 September, Toulouse, France, 2014.
[13] C.M. Roelands, J.H. ter Horst, H.J. Kramer, P.J. Jansens, Analysis of nucleation rate measurements in precipitation processes, Cryst. Growth Des. 6 (6) (2006) 1380–1392.
[14] A. Ruf, J. Worlitschek, M. Mazzoti, Modeling and experimental analysis of PSD measurements through FBRM, Part. Part. Syst. Charact. 17 (2000) 167–179.
[15] Y.S. Jun, B. Lee, G.A. Waychunas, In situ observations of nanoparticle early development kinetics at mineral–water interfaces, Environ. Sci. Technol. 44 (21) (2010) 8182–8189.
[16] D. Darakis, T. Khanam, A. Rajendran, V. Kariwala, T.J. Naughton, A.K. Asundi, Microparticle characterization using digital holography, Chem. Eng. Sci. 65 (2010) 1037–1044.
[17] T. Ooms, W. Koek, J. Westerweel, Digital holographic particle image velocimetry: eliminating a sign-ambiguity error and a bias error from the measured particle field displacement, Meas. Sci. Technol. 19 (2008) 1–14.
[18] S.H. Lee, Y. Roichman, G. Yi, S. Kim, S. Yang, A. Blaaderen, P. Oostrum, D. G. Grier, Characterizing and tracking single colloidal particles with video holographic microscopy, Opt. Express 15 (26) (2007) 18275–18282.
[19] J.W. Mullin, Crystallization, Butterworth-Heinemann, Burlington, MA, 2001.
[20] A.E. Nielsen, Nucleation in barium sulfate precipitation, Acta Chem. Scand. 11 (9) (1957) 1512–1515.
[21] A.E. Nielsen, Homogeneous nucleation in barium sulfate precipitation, Acta Chem. Scand. 15 (2) (1961) 441–442.
[22] R. Mohanty, S. Bhandarkar, B. Zuromski, R. Brown, J. Estrin, Characterizing the product crystals from a mixing tee process, Am. Inst. Chem. Eng. 34 (12) (1988) 2063–2068.
[23] J. Baldyga, J.R. Bourne, Turbulent Mixing and Chemical Reactions, Wiley, Chichester, 1999.
[24] C.P.M. Roelands, R.J.H. Horst, H.J.M. Kramer, P.J. Jansens, Development of an experimental method to measure nucleation rates in reactive precipitation, Cryst. Growth Des. 4 (5) (2004) 921–928.
[25] A.E. Nielsen, The kinetics of crystal growth in barium sulphate precipitation, Acta Chem. Scand. 12 (1961) 1512–1515.
[26] R. Mohanty, S. Bhandarkar, B. Zuromski, R. Brown, J. Estrin, Characterizing the product crystals from a mixing tee process, AIChE J. 34 (12) (1988) 2063–2068.
[27] K. Taguchi, J. Garside, N.S. Tavare, Nucleation and growth kinetics of barium sulphate in batch precipitation, J. Cryst. Growth 163 (3) (1996) 318–328.
[28] R.L. Penn, J.F. Banfield, Imperfect oriented attachment: dislocation generation in defect-free nanocrystals, Science 281 (5379) (1998) 969–971.